Acta Crystallographica Section B
Structural Science
ISSN 0108-7681

Structure of unsolvated magnesium borohydride $Mg(BH_4)_2$

Jae-Hyuk Her,[a]* Peter W. Stephens,[a] Yan Gao,[b] Grigorii L. Soloveichik,[b] Job Rijssenbeek,[b] Matthew Andrus[b] and Ji-Cheng Zhao[b]

[a]Department of Physics and Astronomy, Stony Brook University, Stony Brook, NY 11794-3800, USA, and [b]GE Global Research, Niskayuna, NY 12309, USA

Correspondence e-mail: jher@ic.sunysb.edu

Received 14 March 2007
Accepted 8 May 2007

We have determined the structures of two phases of unsolvated $Mg(BH_4)_2$, a material of interest for hydrogen storage. One or both phases can be obtained depending on the synthesis conditions. The first, a hexagonal phase with space group $P6_1$, is stable below 453 K. Upon heating above that temperature it transforms to an orthorhombic phase, with space group *Fddd*, stable to 613 K at which point it decomposes with hydrogen release. Both phases consist of complex networks of corner-sharing tetrahedra consisting of a central Mg atom and four BH_4 units. The high-temperature orthorhombic phase has a strong antisite disorder in the *a* lattice direction, which can be understood on the basis of atomic structure.

1. Introduction

The search for solid-state hydrogen-storage materials is driving the synthesis of many novel lightweight hydrides. The requirements of high hydrogen content restrict the practical possibilities to hydrides of the lightest dozen or so elements. Magnesium borohydride, $Mg(BH_4)_2$, appears to be a promising material for hydrogen-storage applications. Upon heating, it decomposes to release 14.9 wt % hydrogen (theoretical) according to reaction (1) below (Konoplev & Bakulina, 1971).

$$Mg(BH_4)_2 \rightarrow Mg + 2B + 4H_2 \qquad (1)$$

Although its synthesis was first reported more than 50 years ago (Wiberg & Bauer, 1950), the structure of unsolvated $Mg(BH_4)_2$ remains elusive. Furthermore, the literature data on the synthesis and properties are contradictory, likely because of the presence of different solvates and the difficulty in removing the solvent molecules without decomposition. Plešek and Heřmánek isolated unsolvated magnesium borohydride using the reaction of MgH_2 with diborane (Plešek & Heřmánek, 1966). Konoplev and Bakulina reported the synthesis of unsolvated $Mg(BH_4)_2$ *via* an exchange reaction, and published a qualitative reflection list from X-ray powder diffraction (XRD) data of two crystal modifications (Konoplev & Bakulina, 1971). However, the poor quality of the diffraction data precluded determination of the crystal structure. Empirical calculation of the enthalpy of decomposition of $Mg(BH_4)_2$ (Sarner, 1966; Kuznetsov & Dymova, 1971) gave the very attractive value of ~ 40 kJ mol^{-1} H_2, which would suggest that the hydrogen release should be reversible at moderate temperatures. Interest in this system has stimulated a number of theoretical works, including some predictions of crystal structures (Charkin *et al.*, 1987; Vajeeston *et al.*, 2006; Majzoub & Ozolins, 2006; Bonaccorsi *et al.*, 1991; Nakamori *et al.*, 2006). Unfortunately, these studies all predicted different

Table 1
Experimental and crystallographic details.

	Low-temperature phase	High-temperature phase
Crystal data		
Chemical formula	$Mg(BH_4)_2$	$Mg(BH_4)_2$
M_r	53.99	53.99
Cell setting, space group	Hexagonal, $P6_1$	Orthorhombic, *Fddd* (origin choice: 1)
Data collection temperature	Ambient	Ambient
a, b, c (Å)	10.3414 (4), 10.3414 (4), 37.086 (2)	37.072 (1), 18.6476 (6), 10.9123 (3)
α, β, γ (°)	90, 90, 120	90, 90, 90
Volume (Å^3)	3434.7 (3)	7543.8 (5)
Z	30	64
D_x (Mg m^{-3})	0.78308 (1)	0.76063 (3)
Radiation type	Synchrotron	Synchrotron
Wavelength of incident radiation (Å)	0.70033 (2)	0.69126 (2)
μ (cm^{-1})	1.3925	1.3034
Specimen form, color	Cylinder, white	Cylinder, white
Specimen size (mm)	8 × 1 × 1	8 × 1 × 1
Data collection		
Diffractometer	X16C, NSLS, BNL	X16C, NSLS, BNL
Data collection method	Specimen mounting: rotating glass capillary of 1 mm diameter; mode: transmission; scan method: step	Specimen mounting: rotating glass capillary of 1 mm diameter; mode: transmission; scan method: step
Absorption correction	None	None
2θ (°)	$2\theta_{min}$ = 2.000, $2\theta_{max}$ = 42.000, increment = 0.005	$2\theta_{min}$ = 2.000, $2\theta_{max}$ = 29.175, increment = 0.005
Refinement		
Refinement on	Rietveld method	Rietveld method
R factors and goodness-of-fit	R_p = 0.036, R_{wp} = 0.046, R_{exp} = 0.039, R_B = 0.010, S = 1.187	R_p = 0.025, R_{wp} = 0.031, R_{exp} = 0.027, R_B = 0.0048, S = 1.173
Excluded region(s)	None	None
Profile function	Lorentzian lineshape with computed axial divergence	Lorentzian lineshape with computed axial divergence
No. of parameters	126	82
H-atom treatment	Tetrahedra centered on each B atom	Tetrahedra centered on each B atom
Weighting scheme	$1/\sigma^2$	$1/\sigma^2$
$(\Delta/\sigma)_{max}$	< 0.001	< 0.001
Results		
Mg—B distances (Å)	2.28–2.57	2.34–2.49
B—H distance (Å)	1.12	1.02
Mg—H distances (Å)	> 1.7 (restrained)	> 1.7 (restrained)
Mg thermal parameter	2.37 (5)	6.6 (2)
B thermal parameter	2.4 (1)	10.1 (3)

Computer programs used: *TOPAS*-Academic (Coelho, 2006), *EXPO* (Altomare *et al.*, 1999), *DIAMOND* (Pennington, 1999), *VICS*-II (Momma & Izumi, 2006).

crystal structures for $Mg(BH_4)_2$. It is clear that the validity of thermodynamic predictions and further understanding of this material are dependent upon having a correct crystal structure. In the absence of single crystals suitable for diffraction analysis, we have solved the structures of two phases of $Mg(BH_4)_2$ from powder diffraction data.

2. Experimental

We prepared $Mg(BH_4)_2$ *via* an exchange reaction of $NaBH_4$ with $MgCl_2$ in diethyl ether followed by a desolvation procedure using a modification of the method developed by Konoplev (Konoplev, 1980). The as-synthesized form of $Mg(BH_4)_2$ is critically dependent on the experimental conditions, specifically the final heat treatment. Different procedures can yield either or both of the phases discussed below. Keeping the sample below 453 K results in the formation of the low-temperature (LT) phase, while the high-temperature (HT) phase dominates if the temperature exceeds 508 K. Subsequent cooling does not cause the transformation of the HT phase back to the LT phase. Intermediate temperatures usually give a mixture of both phases. *In situ* synchrotron X-ray powder diffraction experiments revealed that the LT phase undergoes a complete structural transition between 453 and 473 K to the HT phase. Further heating above 573 K led to the decomposition of the sample with the release of hydrogen. DSC measurements on the LT phase indicated an endothermic phase change at 458 K. This feature was absent from measurements started with the HT phase. We describe hereafter LT and HT phases samples annealed at 453 and 508 K, respectively. High-resolution synchrotron powder diffraction experiments showed that the sample after each of these heat treatments was a pure single phase. After heat treatment, each phase was (*meta*)-stable at room temperature for periods of at least several weeks. Holding a sample of the HT phase for several days below the transition temperature did not return the LT phase, attesting to the significant kinetic barriers that make the HT phase metastable at room temperature.

Density measurements for the HT phase were made using a 2 ml pycnometer filled with toluene, and gave a value of 0.76 (3) g cm^{-3} (average of five measurements). Elemental analysis gave an Mg content of 43.6 mol % (45.02 mol % in ideal stoichiometry), which corresponds to 97% purity. The B:Mg ratio was consistently lower than 2 owing to the loss of diborane during the hydrolytic sample preparation for elemental analysis. Attempts to capture the diborane by adding base (*e.g.* amine or ether) during the hydrolysis increased the B:Mg ratio from 1.75–1.8 to 1.9–1.95. Gas analysis during heating of the LT phase from room tempera-

ture to 523 K did not show any gas release, suggesting that the LT to HT transformation is purely structural and does not alter the $Mg(BH_4)_2$ stoichiometry. Full details of the sample preparation, physical properties and hydrogen-storage characteristics will be given in a separate publication.

High-resolution synchrotron powder diffraction patterns were collected at room temperature at the X16C beamline of the National Synchrotron Light Source, Brookhaven National Laboratory. Polycrystalline samples of the LT and HT phases were loaded into thin-walled glass capillaries (1 mm diameter) under inert atmosphere and sealed with vacuum grease. The capillaries were mounted on a goniometer and were kept in constant rotation to ensure an average over many crystallites during the data collection. An Si(111) channel-cut monochromator selected a highly collimated incident X-ray beam. The diffracted X-rays were analyzed by reflection from a Ge(111) crystal and detected by an NaI scintillation counter. Other experimental details and crystallographic information are given in Table 1.

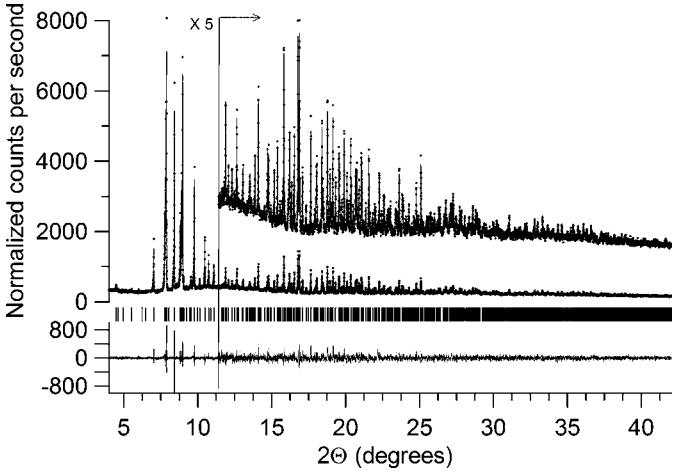

Figure 1
High-resolution synchrotron powder diffraction data (dots), Rietveld fit (line) and allowed Bragg reflections (tick marks) for the LT phase structure of $Mg(BH_4)_2$. The lower trace is the difference, $I_{meas} - I_{calc}$, on the same scale. Note the expanded vertical scale of all traces (including difference) above a scattering angle of 11.4°.

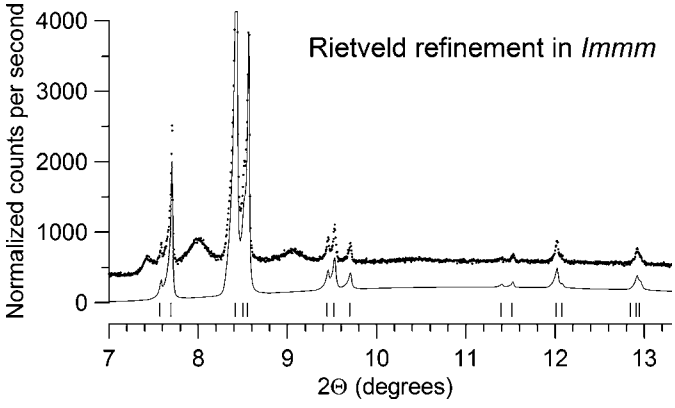

Figure 2
Synchrotron powder diffraction data of the HT $Mg(BH_4)_2$ phase (dots), showing a fit (smooth curve; displaced) and allowed Bragg reflections (tick marks) in *Immm*, which ignores the broad peaks in the diffraction pattern. The model in *Immm* has a cell volume one eighth that of the final structure.

3. Results and structure determination

The diffraction pattern of the LT phase was indexed by *TOPAS*-Academic (Coelho, 2006) as hexagonal and the space group $P6_1$ (or one of its extinction equivalents) was assigned based on systematic absences. A structure solution was found in the space group $P6_1$ (169) by the direct-methods program *EXPO* (Altomare *et al.*, 1999). Rietveld refinement was performed using *TOPAS*-Academic. The quality of the data did not allow the independent refinement of the H atoms, therefore, these were attached to the central B atom and treated as tetrahedral 'rigid' bodies. The B—H bond lengths were all set equal and allowed to vary as a single parameter. Isotropic displacement parameters (IDP) of H atoms were set equal to those of the corresponding B atoms. After the positions of the heavy atoms were refined, the orientations of the BH_4 tetrahedra were first determined by a simulated annealing method implemented in *TOPAS*-Academic and then included in the refinement with the restraint of the minimum Mg—H (1.7 Å) distance. The H atoms are fairly well defined in the final refinement. For example, if all H tetrahedra are replaced by random orientations about each B atom, the weighted profile R factor, R_{wp}, typically increases to 0.049 from its refined value of 0.046 (with all other parameters refined). If allowed to refine, the overall H occupancy is 1.09 (2). (Note that the stated e.s.d.'s are statistical errors reported by *TOPAS*, and are not claimed to be estimates of the precision.) These results should be viewed as supporting the overall picture of the refined structure rather than independent measures of H-atom positions and occupancies. The Rietveld fit is shown in Fig. 1 and refinement results are summarized in Table 1.[1]

Turning now to the annealed HT phase, a portion of its XRD pattern is shown in Fig. 2. Our initial evaluation was that the broad peaks near 7.4, 8 and 9.1° were due to an unknown impurity phase. Using only the sharp peaks, *TOPAS*-Academic indexed a body-centered orthorhombic lattice (a = 18.537, b = 9.325, c = 5.456 Å) with the possible space group $I222$ or one of its extinction equivalents. Both simulated annealing (*TOPAS*-Academic) and direct methods (*EXPO*) programs suggested similar structure models in the space group *Immm*. We could obtain a satisfactory Rietveld refinement to the powder diffraction data (R_{wp} = 0.0305) fitting the various broad features as individual pseudo-Voigt peaks (not shown in Fig. 2), but the refined structure suffered from some serious flaws. Several sites refined to fractional occupancies of the order of a half and many of these half-occupied sites were unreasonably close to one another. However, this model in *Immm* had the correct density ($\sim$ 0.7 g cm^{-3}), and produced a

[1] Supplementary data for this paper are available from the IUCr electronic archives (Reference: LM5009). Services for accessing these data are described at the back of the journal.

fit of sufficient quality (shown in Fig. 2, vertically displaced) that it could not be dismissed out of hand.

This result suggested that our *Immm* model was only an average structure and that the partially occupied sites might be correlated to produce a larger unit cell without the occupancy of sites that were unreasonably close. Such correlations could produce diffuse scattering and we hypothesized that this might be the cause of the broad 'impurity' lines shown in Fig. 2. Searching for possible superlattices, we discovered that the broad peaks could be indexed as (odd, odd, odd) reflections if the original *Immm* cell was doubled in each direction. However, to explain the broadening of only the odd order peaks, we hypothesized an idealized face-centered orthorhombic structure with significant antisite disorder. Only a limited number of possible extensions of the original *Immm* model to a face-centered superlattice exist and we found satisfactory agreement with the relative intensities of the odd-order peaks in *Fddd*. The crystallographic data of this phase is summarized in Table 1.

In the $2 \times 2 \times 2$ face-centered cell, the three clear broad peaks in Fig. 2 are (131), (331) and (531) located about 7.4, 8 and 9.1°, respectively. Other odd-order peaks are observed, but they are significantly weaker and/or broader than those three. It is immediately seen that the width of odd-order peaks increases rapidly with increasing Miller index h, which led us to hypothesize that the antisite disorder occurs across domain walls perpendicular to the orthorhombic a axis. Fig. 3 illustrates the basic concept in two dimensions, for a centered rectangular lattice consisting of two types of atoms. Define an order parameter Φ which is equal to 1 in a domain where the filled circles are located at fractional coordinates (0, 0) and ($\frac{1}{2}$, $\frac{1}{2}$); $\Phi = -1$ in a domain where the filled circles are located at (0, $\frac{1}{2}$) and ($\frac{1}{2}$, 0). The scattering amplitudes from unit cells in the two domains are in-phase for even-order reflections, and out-of-phase for odd-order reflections. Therefore, all even-order reflections are sharp and odd-order reflections consist of streaks perpendicular to the domain wall direction. The length of the streaks is inversely proportional to the average distance between the domain walls.

In the case of the three-dimensional structure of $Mg(BH_4)_2$, we use origin choice 1 of the *Fddd* space group (Hahn, 1996), and again define an order parameter Φ to track the local site occupancy of the atoms that were half-occupied in the *Immm* model of the average structure. Φ is defined to be +1 in a region where atoms are located at fractional coordinates generated by (x, y, z), $(-x, -y, z)$, $(-x, y, -z)$, $(\frac{1}{4} - x, \frac{1}{4} - y, \frac{1}{4} - z)$ *etc.*, and $\Phi = -1$ where atoms are located at $(x, y, z + \frac{1}{2})$, $(-x, -y, z + \frac{1}{2})$, $(-x, y, \frac{1}{2} - z)$, $(\frac{1}{4} - x, \frac{1}{4} - y, \frac{3}{4} - z)$ *etc*. If random site disorder occurs at planes perpendicular to the a axis, the correlation function of Φ will be

$$\langle \Phi(0)\Phi(\mathbf{r}) \rangle = \exp(-|\mathbf{r} \cdot \hat{\mathbf{x}}|/\xi),$$

where ξ is the correlation length. This leads to diffraction peaks with intrinsic shape[2]

$$S(\mathbf{Q}) = \sum_{h,k,l} |A(hkl)|^2 \delta(Q_x - ha^*)\delta(Q_y - kb^*)\delta(Q_z - lc*)$$

for h, k, l even, and

$$S(\mathbf{Q}) = \sum_{h,k,l} |A(hkl)|^2 \left(\frac{1/\pi\xi}{(Q_x - ha^*)^2 + \xi^{-2}} \right) \delta(Q_y - kb^*)\delta(Q_z - lc^*)$$

for h, k, l odd, where $A(hkl)$ is the amplitude of the (hkl) diffraction peak. Note that the peaks have a Lorentzian lineshape in the direction perpendicular to the planes that separate the domains of the site disorder. Line-shape fits were able to exclude the possibility that the direction of the primary peak broadening is along b^* or c^*, or that the odd-order peaks are simply strain broadened, with width proportional to Q.

In a powder diffraction experiment, the projected HWHM (half width at half-maximum) of the odd-order peaks along the magnitude of Q is given by $ha^*/\xi Q$. The FWHM (full width at half-maximum) in 2θ is then $(\lambda^2/a\pi \sin 2\theta)h/\xi$. The facility for *TOPAS*-Academic to include symbolic algebra allows us to model that lineshape and refine the correlation length ξ to ~ 20 Å, which is half the a lattice parameter. The shortest length of a coherent domain is $a/4$ because the structure admits domain walls at $x = 0$, $\frac{1}{4}$, $\frac{1}{2}$ or $\frac{3}{4}$. Consequently, the

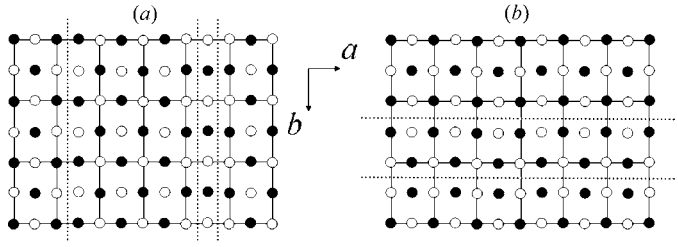

Figure 3
(*a*) Illustrative centered rectangular lattice with two kinds of atoms: filled and open circles. The thin lines represent the unit cell. Randomly spaced antiphase domains are separated by walls perpendicular to the a axis. (*b*) Antiphase domain walls are perpendicular to the b axis.

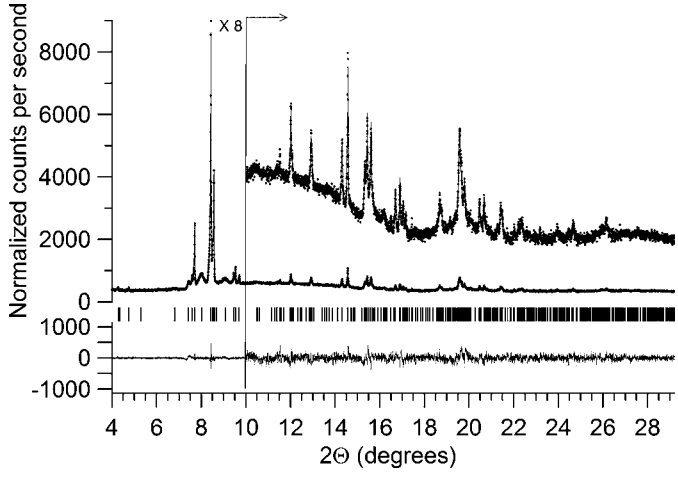

Figure 4
High-resolution synchrotron powder diffraction data (dots), Rietveld fit (line) and allowed Bragg reflections (tick marks) for the HT $Mg(BH_4)_2$ phase. The lower trace is the difference, $I_{meas} - I_{calc}$, on the same scale. Note the expanded vertical scale for all traces (including difference) above 10° scattering angle.

[2] We are using the physicists' convention of $Q = 4\pi \sin(\theta)/\lambda$, $a^* = 2\pi/a$.

stacking of domains in the *a* direction must be regarded as nearly random. The *Fddd* structure must therefore be taken as an idealization of the physical structure. The Rietveld fit, including the antisite disorder, is shown in Fig. 4.

We attempted to locate H atoms in the HT phase by simulated annealing starting from a refined heavy-atom structure, similar to our treatment of the LT phase. However, the H atoms in the HT phase are not nearly as well defined because the sample diffracted with much poorer resolution, evidently owing to the substantially higher thermal parameters for all atoms. We have defined BH_4 tetrahedra as rigid bodies centered at each B atom, and refined their orientations subject to the restraints of minimum B—H (1.0 Å) and Mg—H (1.7 Å) distances. The difference between refined and random orientations of H tetrahedra about each B atom (R_{wp} = 0.0311 *versus* 0.0316) is not significant. For the sake of completeness, we have included the H atoms in our refinement and coordinates, but they should not be regarded as being determined by the diffraction data. Neutron diffraction would be better able to detect H positions (Fossdal *et al.*, 2005; Chater *et al.*, 2006), but the presence of incoherently scattering H and strongly absorbing B would make the experiment difficult without a sample isotopically enriched with 2D and 11B.

4. Discussion

The structures of both phases of magnesium borohydride, $Mg(BH_4)_2$, consist of corner-sharing tetrahedra with Mg atoms[3] at the center and BH_4 units at the vertices. The structures of the LT and HT phases are illustrated in Figs. 5 and 6, respectively. The H atoms are more clearly observed in the LT phase than the HT phase; in the latter, we have included them in the refinement largely guided by chemical intuition based on known structures of borohydride complexes. Despite the evolution of one from the other upon heating and the similarities in lattice parameters, we could not discern a clear relationship between the connectivities of the two phases.

The LT (hexagonal) phase has a complicated structure with five distinct types of MgB_4 tetrahedra. Mg3 are located close to the *c* axis, while the other four Mg atoms are relatively close to the *ab* planes. No two Mg atoms of the same type share a BH_4 bridge. With only two Mg sites, the HT (orthorhombic) phase has a simpler description. Mg1 tetrahedra have one face that is nearly parallel to the *bc* plane, whereas Mg2 tetrahedra have one edge nearly parallel to *a* and one edge nearly parallel to *c*. Each type of Mg tetrahedron is bonded to one tetrahedron of the same type, and three tetrahedra of the opposite type.

We next discuss the local connections and shapes of the MgB_4 tetrahedra. In the LT phase, Mg—Mg distances of linked tetrahedra range from 4.60 to 4.88 Å, and the Mg—B—Mg angles range from 145 to 174°. Those of the HT phase are similar, but vary over a smaller range (4.61–4.72 Å, 150–171°). In discussing the distortions from ideal tetrahedral geometry, it is interesting to compare the MgB_4 tetrahedra with those more commonly found in oxide materials. Robinson *et al.* (1971) defined separate measures of bond length and angular distortions from ideal tetrahedra (and octahedra) and found that the two measures were closely correlated for a wide variety of oxides. We have computed those parameters for the MgB_4 tetrahedra in the two phases considered here, and present the results in Fig. 7. In this figure, the trend line from Robinson *et al.* is drawn, over the entire range of tetrahedral oxides listed therein. The tetrahedra in the HT phase are essentially undistorted in comparison with most oxide materials, whereas the tetrahedra in the LT phase are much more distorted relative to any observed oxide. Nevertheless, the linear relationship between measures of distortion noted by

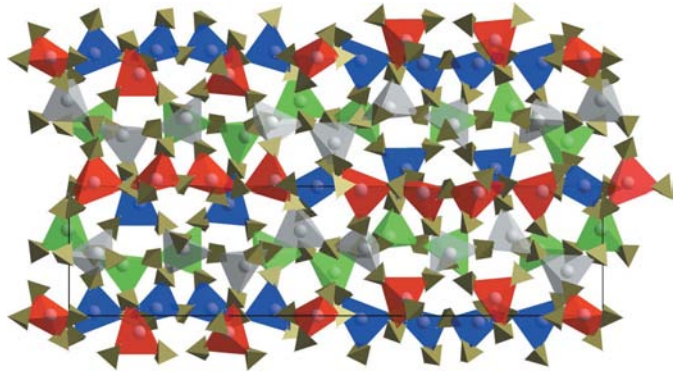

Figure 5
Structure of the LT $Mg(BH_4)_2$ phase in space group $P6_1$ viewed along the hexagonal *a* axis, showing two unit cells. The small opaque tetrahedra are BH_4 units; the larger (partially transparent) tetrahedra represent Mg and the four nearest B atoms. MgB_4 tetrahedra are colored according to their projection along *a*; units centered near 0, $\frac{1}{4}$, $\frac{1}{2}$, and $\frac{3}{4}$ are colored red, green, blue and grey, respectively.

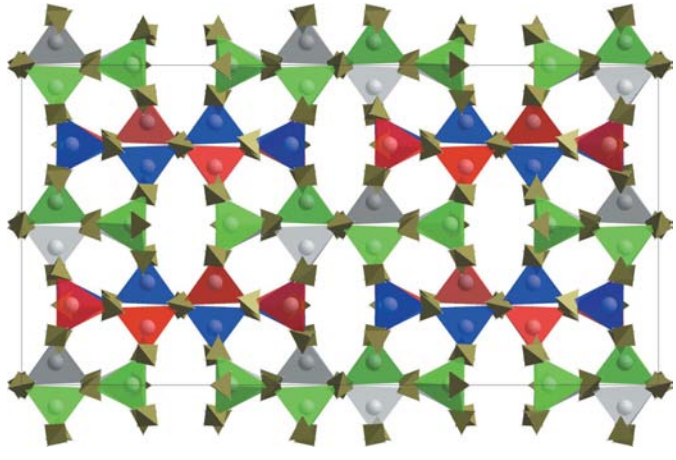

Figure 6
Structure of the HT $Mg(BH_4)_2$ phase in the space group *Fddd* viewed along the *c* axis. This is an idealized view that omits the strong antisite disorder discussed in the text. Small opaque tetrahedra are BH_4 units; MgB_4 tetrahedra are colored according to their position along *c*; units centered near 0, $\frac{1}{4}$, $\frac{1}{2}$, and $\frac{3}{4}$ are colored red, green, blue and grey, respectively.

[3] It is likely that there is some charge transfer between Mg and BH_4 units in these two phases. However, in the absence of direct information about ionization state, we prefer to use the word atom rather than ion.

Table 2
Bonding in selected borohydrides.

	Ionic radius† (Å)	Coordinating BH_4 groups	M—B (Å)	Coordinating H atoms
Be	0.27‡	3	1.92–2.00	6
Mg (LT)	0.57‡	4	2.28–2.57	8
Mg (HT)	0.57‡	4	2.34–2.49	8
Li§	0.59‡	4	2.47–2.54	9
Ca	1.00¶	6	2.91–2.98	12
Na§	1.02¶	6	3.07	12
K§	1.37¶	6	3.35	12

† Ionic radii from Shannon (1976). ‡ IV coordination. § Room-temperature structure ¶ VI coordination.

Robinson *et al.* extends approximately to these much softer $Mg(BH_4)_2$ units. The reduced tetrahedral distortion from the LT to the HT phase as shown in Fig. 7 may be partly responsible for the irreversible phase transition upon heating.

Scrutiny of the HT crystal structure (Fig. 6) offers an explanation of the particular antisite disorder observed. As discussed above, an ideal lattice for this phase would be F-centered orthorhombic, but the odd-order diffraction peaks are broadened in the a^* direction of the reciprocal lattice, indicating that the structure is coherent over long distances in the bc planes, but sustains frequent defects in the a direction, which are equivalent to displacements by half of the a lattice parameter. Fig. 8 shows two views of the HT structure with phase jumps perpendicular to the a and b axes. Fig. 8(*a*) shows that a shift by half a unit cell perpendicular to the a axis does not violate the pattern of corner-connected tetrahedra. Similar shifts perpendicular to the b axis (Fig. 8*b*) and c axis (not shown) yield tetrahedra that would be unfavorably forced to share edges and have two different orientations co-exist on the domain wall, in contrast to the rest of the structure. (Other locations of the domain wall within the unit cell are equally unfavorable.) As a consequence, planar antiphase boundaries perpendicular to the a axis are strongly favored relative to other directions, and explain the observed broadening of the superlattice reflections discussed above.

The correlation length of less than a full lattice translation suggests that the antiphase defects in the a direction occur very frequently. Consequently, they must have a very low energy and we believe that they are probably intrinsic to the orthorhombic phase. Attempts to anneal the defects out of the structure by heating over prolonged times at 493 K, followed by slow cooling to room temperature, did lead to some shar-

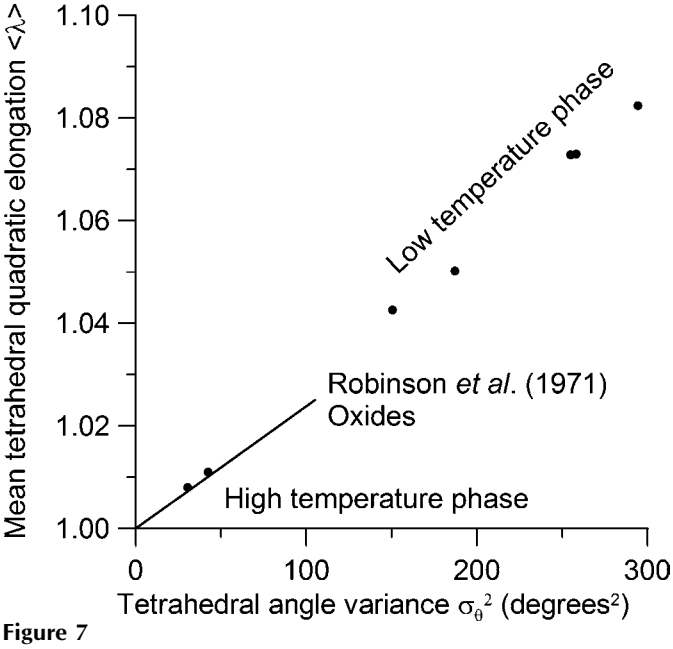

Figure 7
Degrees of distortion of MgB_4 tetrahedra from ideal tetrahedral geometry for the two phases described in this work. Definitions and numerical values are given in the supplementary information. Separate symbols are plotted for each of the independent units in each structure. The diagonal line illustrates the range and correlation of oxide materials studied by Robinson *et al.* (1971).

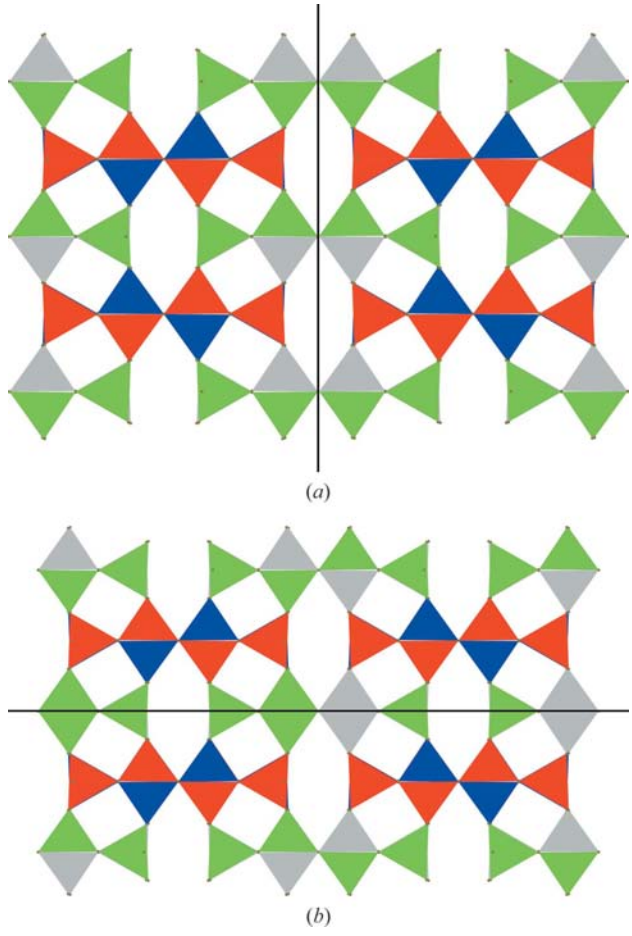

Figure 8
(*a*) View of the HT (*Fddd*) structure of $Mg(BH_4)_2$ with a phase jump perpendicular to the a axis. The left side has the same lattice occupancy as shown in Fig. 6 (order parameter $\Phi = 1$ as defined in text), while the right side is shifted by half a unit cell ($\Phi = -1$). Tetrahedra are colored according to their position along the c axis, as defined in Fig. 6. (*b*) View with a phase jump perpendicular to the b axis. The top has $\Phi = 1$ and the bottom has $\Phi = -1$. H atoms are omitted for clarity. Thin black lines represent the antiphase domain boundary.

pening of the broad peaks, but a substantial degree of disorder remained.

The complexity and enormous sizes of these unit cells are a departure not only from theoretical predictions, but also from the relatively simple CdI_2-type unit cell of compositionally similar $Mg(AlH_4)_2$ (Fichtner *et al.*, 2003; Fossdal *et al.*, 2005) and other borohydrides such as ABH_4 (A = Li, Na and K; Abrahams & Kalnajy, 1954; Soulié *et al.*, 2002; Renaudin *et al.*, 2004) or $M(BH_4)_2$ (M = Be and Ca; Lipscomb & Marynick, 1971; Marynick & Lipscomb, 1972; Miwa *et al.*, 2006). Comparison of these structures shows that $Mg(BH_4)_2$ takes an intermediate position between the purely ionic borohydrides (Na, K and Ca) and those with more covalent character (Li and Be; Table 2). The larger alkali metal borohydrides, ABH_4 (A = Na and K), crystallize in a rock-salt structure with metal atoms octahedrally coordinated to six BH_4 tetrahedra (Abrahams & Kalnajy, 1954; Renaudin *et al.*, 2004). Similarly, in $Ca(BH_4)_2$ the Ca atom is coordinated by six BH_4 units forming an elongated octahedron, with all the B—Ca—B angles around 90° (Miwa *et al.*, 2006). In each case, the metal atom is bound to 12 H atoms, two from each of the six surrounding BH_4 groups.

The smaller, less electropositive cations (Be and Li) show lower coordination numbers. In $Be(BH_4)_2$ the Be atom is coordinated by only three BH_4 units, one terminal and two bridging, *via* two H atoms each (Lipscomb & Marynick, 1971; Marynick & Lipscomb, 1972). In contrast to the *f.c.c.* structures of the alkali metals above, the crystal structure of $LiBH_4$ is orthorhombic (at room temperature) and has distorted BH_4 tetrahedra (Soulié *et al.*, 2002). The Li atom is coordinated by four BH_4 units, *via* nine H atoms. This is similar to the coordination we observed for the Mg atom in both phases of $Mg(BH_4)_2$, wherein the Mg atoms form corner-sharing Mg-4(BH_4) tetrahedra. Each Mg is coordinated to two H atoms from each BH_4 group (Strictly speaking, the final conclusion on the hydrogen configuration must be postponed until good-quality neutron data are available, since there are too many parameters to uniquely locate the H atoms with only X-ray powder diffraction data.) Thus, as the ionic radius and the ionic character of the metal are increased (moving down Table 2), the number of coordinating BH_4 groups increases from 3 to 4 to 6. $Mg(BH_4)_2$ falls in line with this trend. Why the structure is so much more complicated than that of $Mg(AlH_4)_2$ remains to be explained, but is likely due to the more covalent nature of the BH_4 unit *versus* AlH_4.

5. Conclusion

Our study of $Mg(BH_4)_2$ was motivated by its potential as a hydrogen-storage material. Knowledge of its structure is a necessary first step in understanding its hydrogen desorption properties and finding a practical means of regenerating it. As synthesized, unsolvated $Mg(BH_4)_2$ adopts the low-temperature (LT) structure. Heating above 453 K yields the higher-symmetric high-temperature (HT) modification, which is metastable at room temperature. Both phases consist of complex networks of corner-sharing MgB_4 tetrahedra, with four H atoms associated with each B. The LT phase has a hexagonal structure with 30 formula units per unit cell and five distinct Mg sites. The HT phase has an orthorhombic structure, with two independent Mg sites and 64 formula units per unit cell. The latter phase has significant disorder, which may be explained by the formation of antiphase domain walls parallel to the crystallographic *bc* plane.

We have observed evidence for at least one other modification depending on the experimental conditions. Perhaps this is not surprising given the varied motifs accessible by linking Mg-4(BH_4) tetrahedra. Although structurally related to other borohydrides in many ways, the complexity and large units cells of $Mg(BH_4)_2$ are a surprising twist to an already fascinating material.

Note added in proof. The structure of the LT phase has been independently determined by Cěrny, R., Filinchuk, Y., Hagemann, H. & Yvon, K. (2007). *Angew. Chem. Int. Ed.* In the press.

Use of the National Synchrotron Light Source, Brookhaven National Laboratory, was supported by the US Department of Energy (DOE), Office of Science, Office of Basic Energy Sciences, under Contract No. DE-AC02-98CH10886. Part of the work was supported by DOE, Office of Energy Efficiency and Renewable Energy, under Contract No. DE-FC3605GO15062 as part of the DOE Metal Hydride Center of Excellence.

References

Abrahams, S. C. & Kalnajy, J. (1954). *J. Chem. Phys.* **22**, 434–436.
Altomare, A., Burla, M. C., Camalli, M., Carrozzini, B., Cascarano, G. L., Giacovazzo, C., Guagliardi, A., Moliterni, A. G. G., Polidori, G. & Rizzi, R. (1999). *J. Appl. Cryst.* **32**, 339–340.
Bonaccorsi, R., Charkin, O. P. & Tomasi, J. (1991). *Inorg. Chem.* **30**, 2964–2969.
Charkin, O. P., Bonaccorsi, R., Tomasi, J., Zyubin, A. S. & Gorbik, A. A. (1987). *Zh. Neorg. Khim.* **32**, 2644–2648.
Chater, P. A., David, W. I. F., Johnson, S. R., Edwards, P. P. & Anderson, P. A. (2006). *Chem. Commun.* **23**, 2439–2441.
Coelho, A. A. (2006). *TOPAS-Academic.* http://members.optusnet.-com.au/~alancoelho.
Fichtner, M., Engel, J., Fuhr, O., Gloess, A., Rubner, O. & Ahlrichs, R. (2003). *Inorg. Chem.* **42**, 7060–7066.
Fossdal, A., Brinks, H. W., Fichtner, M. & Hauback, B. C. (2005). *J. Alloy Compd.* **387**, 47–51.
Hahn, T. (1996). Editor. *International Tables for Crystallography*, Vol. A, 4th Ed. Dordrecht: Kluwer Academic Publishers.
Konoplev, V. N. (1980). *Russ. J. Inorg. Chem.* **25**, 964–966.
Konoplev, V. N. & Bakulina, V. M. (1971). *Izv. Akad. Nauk SSSR Ser. Khim.* **1**, 159–161.
Kuznetsov, V. A. & Dymova, T. N. (1971). *Russ. Chem. Bull.* **20**, 204–208.
Lipscomb, W. N. & Marynick, D. S. (1971). *J. Am. Chem. Soc.* **93**, 2322–2323.
Majzoub, E. H. & Ozolins, V. (2006). Abstract in MH2006, International Symposium on Metal–Hydrogen Systems. Maui, Hawaii, p. 12.
Marynick, D. S. & Lipscomb, W. N. (1972). *Inorg. Chem.* **11**, 820–823.
Miwa, K., Aoki, M., Noritake, T., Ohba, N., Nakamori, Y., Towata, S., Züttel, A. & Orimo, S. (2006). *Phys. Rev. B*, **74**, 155122.

Momma, K. & Izumi, F. (2006). *VICS*-II. http://www.geocities.jp/kmo_mma/crystal/en/vics.html.
Nakamori, Y., Miwa, K., Ninomiya, A., Li, H., Ohba, N., Towata, S., Züttel, A. & Orimo, S. (2006). *Phys. Rev. B*, **74**, 045126.
Pennington, W. T. (1999). *J. Appl. Cryst.* **32**, 1028–1029.
Plešek, J. & Heřmánek, S. (1966). *Collect. Czech. Chem. Commun.* **31**, 3845–3858.
Renaudin, G., Gomes, S., Hagemann, H., Keller, L. & Yvon, K. (2004). *J. Alloys Compd.* **375**, 98–106.
Robinson, K., Gibbs, G. V. & Ribbe, P. H. (1971). *Science*, **172**, 567–570.
Sarner, S. F. (1966). *Propellant Chemistry*, 1st Ed. New York: Reinhold Publishing Corporation.
Shannon, R. D. (1976). *Acta Cryst.* A**32**, 751–767.
Soulié, J.-Ph., Renaudin, G., Černý, R. & Yvon, R. K. (2002). *J. Alloys Compd.* **346**, 200–205.
Vajeeston, P., Ravindran, P., Kjekshus, A. & Fjellvag, H. (2006). *Appl. Phys. Lett.* **89**, 071906.
Wiberg, E. & Bauer, R. (1950). *Z. Naturforsch. B*, **5**, 397.